Journal of Materials Chemistry A

COMMUNICATION

View Article Online
View Journal | View Issue

Cite this: J. Mater. Chem. A, 2016, 4, 2413

Received 11th December 2015
Accepted 15th January 2016

DOI: 10.1039/c5ta10102f

www.rsc.org/MaterialsA

Functionalized graphene quantum dots as a novel cathode interlayer of polymer solar cells†

Zicheng Ding,[a] Zhongshuo Miao,[ab] Zhiyuan Xie[a] and Jun Liu*[a]

The cathode interlayer (CIL) plays an important role in maximizing the photovoltaic efficiency of polymer solar cells (PSCs). The principle to design organic/polymeric CIL materials is to functionalize π-conjugated skeletons with specific polar/ionic groups. Here, using the principle of organic/polymer CIL materials, we developed graphene quantum dots functionalized with tetramethylammonium at the edge (**GQDs-TMA**) to be used as a CIL for PSCs with good device performance. The peripheral tetramethylammonium groups can form an interfacial dipole with the cathode to decrease the work function. Graphene quantum dots are used as the π-conjugated skeleton because of their facile synthesis, high conductivity and good film-forming capability. As a result, using an active layer of **PCDTBT**:**PC_{71}BM**, a power conversion efficiency (PCE) of 7.01% is achieved with **GQDs-TMA** as the CIL, much higher than that (<6.5%) with Ca, LiF, or ZnO as the CIL. PSCs with a conventional configuration using **GQDs-TMA** as the CIL and PTB7-Th:**PC_{71}BM** as the active layer show a PCE of 8.80%, which is the highest reported so far for PSCs containing graphene materials. Moreover, **GQDs-TMA** can also work well when high work function metals (*e.g.* Ag, Au) are used as the cathode. To the best of our knowledge, this is the first report on solution-processed graphene derivatives as a CIL with excellent PSC device performance.

1. Introduction

Polymer solar cells (PSCs) are an emerging renewable energy technology with the great advantages of low cost, flexibility and light weight.[1–3] In the past decade, tremendous efforts have been devoted to the development of anode interlayers (AILs) and cathode interlayers (CILs) to improve the efficiency and stability of PSCs.[4–7] The CIL materials can be low work function metals (*e.g.* Ca, Ba), inorganic salts (*e.g.* LiF, Cs_2CO_3), inorganic semiconducting oxides (*e.g.* TiO_2, ZnO) and organic molecules/polymers. Among them, organic molecules/polymers are of particular interest owing to their advantages of low-temperature solution processing and good contact with the active layer.[8–12] The principle to design organic/polymeric CIL materials is to functionalize π-conjugated skeletons with specific polar/ionic groups, such as amino, ammonium, zwitterions, phosphonate, *etc.* The polar/ionic groups form an interfacial dipole with the cathode to lower the cathode work function and to improve electron extraction.[13] The π-conjugated skeletons also play an important role in organic/polymer CIL materials. By replacing typical p-type polymers with new n-type molecules/polymers as the π-conjugated skeletons, scientists have developed thickness-insensitive CIL materials, which is compatible with the roll-to-roll process required for mass production of large-area PSCs.[14–17] However, the high-efficiency organic/polymer CIL materials suffer from tedious multi-step synthesis, which is undesirable for their production and practical application.[10–12,14–17] Developing novel CIL materials using the same principle but with simple synthesis is an important topic.

Solution-processable graphene derivatives have been demonstrated to be a new class of AIL and CIL materials for PSCs.[18] The chemical structures of the graphene derivatives can be modified and their properties can be tuned to meet the multiple requirements of the AIL. For example, we have developed graphene oxide (GO), graphene oxide ribbon (GOR) and graphene quantum dots (**GQDs**) to be used as the AIL.[19–22] Zhang *et al.* and Na *et al.* have prepared functionalized GO derivatives with high work function to be used as the AIL in high-performance PSCs.[23,24] However, CIL materials based on solution-processable graphene derivatives are rare.[19,25,26] Moreover, they always exhibit poor device performance probably due to the incomplete functionalization of graphene derivatives to decrease the work function and the poor film-forming properties of graphene sheets. In addition, **GQDs** have been used in the active layer of PSCs.[27,28]

[a]State Key Laboratory of Polymer Physics and Chemistry, Changchun Institute of Applied Chemistry, Chinese Academy of Sciences, Changchun 130022, P. R. China. E-mail: liujun@ciac.ac.cn

[b]University of Chinese Academy of Sciences, Beijing 100039, P. R. China

† Electronic supplementary information (ESI) available: Characterization of **GQDs-TMA**, UV-vis spectra, TGA curve, conductivity, *J–V* plots in the dark and EQE curves of different systems with various cathodes. See DOI: 10.1039/c5ta10102f

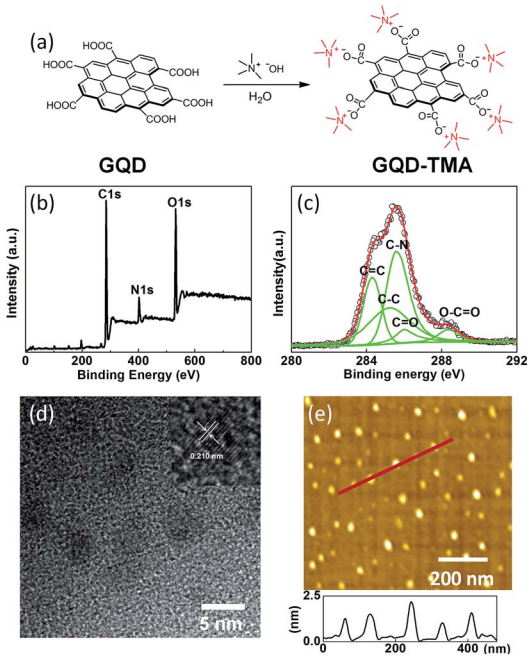

Fig. 1 (a) Synthetic route of **GQDs-TMA**. (b) XPS survey spectrum and (c) XPS C 1s spectrum of **GQDs-TMA**. (d) TEM image and (e) AFM image of **GQDs-TMA**. The inset of (d) is a representative high-resolution TEM image of individual **GQDs-TMA**. The bottom of (e) is the height profile corresponding to the line shown in the AFM image.

Here, adopting the principle of organic/polymer CIL materials, we developed graphene quantum dots functionalized with tetramethylammonium at the edge (**GQDs-TMA**) to be used as the CIL for PSCs with good device performance. Fig. 1a shows the schematic illustration of the chemical structure of **GQDs-TMA**. The peripheral tetramethylammonium groups can form an interfacial dipole with the cathode to decrease the work function. **GQDs** are used as the π-conjugated skeleton because of their facile synthesis and good film-forming capability.[22] As a result, **GQDs-TMA** can work well as the CIL irrespective of the cathode materials (*e.g.* Al, Ag, Au). With Al as the cathode, **GQDs-TMA** outperform the widely used CIL materials, including Ca, LiF, or ZnO and demonstrates a PCE of 8.80%. To the best of our knowledge, this is the first report on solution-processed graphene derivatives as a CIL with excellent PSC device performance.

2. Results and discussion

As shown in Fig. 1a, **GQDs-TMA** were synthesized by simple neutralization of **GQDs** with $(CH_3)_4N^+\cdot OH^-$ in aqueous solution. **GQDs** were prepared by chemical oxidation of carbon black with HNO_3/H_2SO_4 as reported previously.[22] The **GQDs** have a high content of COOH groups at the edge and negligible content of epoxy/hydroxy groups on the basal plane of the graphene structure.[22] With the addition of basic $(CH_3)_4N^+\cdot OH^-$ to an aqueous solution of **GQDs**, the acidic COOH groups of **GQDs** are converted to $COO^-\cdot(CH_3)_4N^+$ to give **GQDs-TMA**. The simple synthesis methodology indicates that **GQDs-TMA** can be synthesized on a large scale with high yield. **GQDs-TMA** show good solubility (>10 mg mL^{-1}) in water and polar organic solvents, such as methanol and acetone. Moreover, **GQDs-TMA** are insoluble in non- or low-polarity organic solvents, such as hexane, toluene, chlorobenzene and *o*-dichlorobenzene. The solubility of **GQDs-TMA** makes them suitable for multilayer PSCs processed with orthogonal solvents.

According to the X-ray photoelectron spectroscopy (XPS) survey spectrum (Fig. 1b), the content of nitrogen in **GQDs-TMA** is 8.94 at%. The band at 285.6 eV assigned to C–N groups in the XPS C 1s spectrum (Fig. 1c) confirms the presence of nitrogen species in **GQDs-TMA**. The presence of the band at 288.3 eV (attributed to COO^- groups) and the absence of the band at 288.8 eV (attributed to COOH groups) indicate that all the peripheral COOH groups in **GQDs** have been transformed to $COO^-\cdot(CH_3)_4N^+$ groups in **GQDs-TMA**. As shown in Fig. 1d, the transmission electron microscopy (TEM) image suggests that **GQDs-TMA** have a uniform lateral size of *ca.* 4 nm. The inset of Fig. 1d reveals an in-plane lattice fringe of 0.210 nm assigned to the (102) facet of sp^2 graphitic carbon.[29] The size and the lattice structure of **GQDs-TMA** are similar to those of **GQDs**, indicating that the introduction of TMA groups does not affect the basal plane of **GQDs**. The height profile of the atomic force microscopy (AFM) image (Fig. 1e) shows that the thickness of **GQDs-TMA** is *ca.* 1–2 nm, indicating single- or two-layered graphene

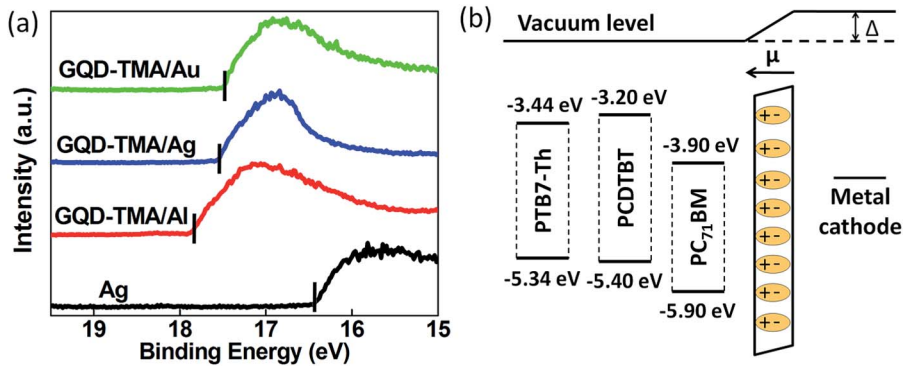

Fig. 2 (a) The secondary electron cutoff region in UPS spectra of the **GQDs-TMA** interlayer on Al, Ag and Au. (b) Energy level diagram of the PSC devices based on **PCDTBT**:PC_{71}**BM** and PTB7-Th:PC_{71}**BM** active layers with the **GQD-TMA** cathode interlayer.

structure.[30] The UV-vis absorption spectrum of **GQDs-TMA** in aqueous solution (Fig. S1†) exhibits an absorption peak at 227 nm with negligible absorbance in the visible and near-infrared range. The transparency in the visible and near-infrared range of **GQDs-TMA** is beneficial for their application as a CIL in PSCs.

The key requirement of CIL materials is their ability to produce an interfacial dipole to induce a vacuum-level shift and lower the electrode work function. To investigate the effect of **GQDs-TMA** on the work function of different electrodes, including Al ($\phi = 4.3$ eV), Ag ($\phi = 4.7$ eV) and Au ($\phi = 5.1$ eV), ultraviolet photoelectron spectroscopy (UPS) is used. Fig. 2a displays the secondary electron cutoff region in UPS spectra of the **GQD-TMA** interlayer on Al, Ag and Au. After a thin layer of **GQDs-TMA** is deposited on the surface of the metals, the work function changes to 3.3 eV, 3.6 eV and 3.7 eV for Al, Ag and Au, respectively. The reason for the decreased work function may be due to the formation of an interfacial dipole at the metal interface, which has been reported for many organic/polymer CIL materials with amine/ammonium functional groups.[8,13] With the **GQD-TMA** layer, different metals lead to different work function decrease possibly due to the different tilt angles and densities of the dipole moment of **GQDs-TMA** on the metal surfaces.[31,32] This phenomenon is common for many organic/polymeric CIL materials.[13,17,33] In PSCs, the low work function of metal cathodes allows them to form an ohmic contact with the **$PC_{71}BM$** acceptor in the active layer (Fig. 2b). Moreover, the low cathode work function would result in the large built-in potential across the PSC device, which is beneficial for good device performance. The conductivity of **GQDs-TMA** (Fig. S3†) is measured to be 6×10^{-8} S cm^{-1}, which is nearly one order of magnitude higher than that (7×10^{-9} S cm^{-1}) of the widely used CIL material PFN with amino groups tethered to the polyfluorene backbone.[17,34] The relatively high conductivity of **GQDs-TMA** may result from the preservation of graphene lattice in their basal plane.[35] Moreover, the high conductivity of **GQDs-TMA** is expected to reduce the series resistance (R_S) of PSC devices.

The decreased cathode work function, high conductivity and good transparency motivate us to incorporate **GQDs-TMA** as the CIL for PSCs. At first, we fabricated single-junction PSC devices with a conventional configuration using different CILs. The device configuration is ITO/PEDOT:PSS/poly[*N*-9-hepta-decanyl-2,7-carbazolealt-5,5-(4′,7′-di-thienyl-2′,1′,3′-benzothiadiazole)] (**PCDTBT**):[6,6]-phenyl C71-butyric acid methyl ester (**$PC_{71}BM$**)/CIL/Al (Scheme 1). The CIL materials are none, LiF, Ca, ZnO or **GQDs-TMA**. The **GQDs-TMA** are spincoated on top of the active layer from their MeOH solution. The current density–voltage (*J*–*V*) plots of the devices are shown in Fig. 3a and the corresponding device parameters are summarized in Table 1. The device with bare Al and without any CIL shows an open-circuit voltage (V_{OC}) of 0.83 V, short-circuit current density (J_{SC}) of 9.82 mA cm^{-2}, fill factor (FF) of 59.45%, corresponding to PCE of 4.85%. With a normal CIL of LiF, Ca or ZnO used in the PSC devices, the V_{OC}, FF and J_{SC} all increase. As a result, PCEs in the range from 6.20% to 6.49% are obtained, which are consistent with the results reported for PSCs based on the **PCDTBT:PC_{71}BM** active layer.[36,37] In comparison, the device with **GQD-TMA** as

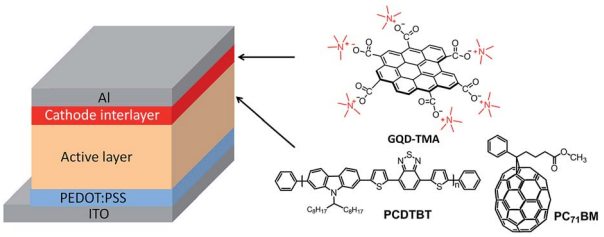

Scheme 1 Device structure of the PSC devices based on the PCDTBT:PC_{71}BM active layer with a GQD-TMA cathode interlayer. The schematic illustration of the chemical structure of GQDs-TMA is also shown.

CIL shows increased V_{OC} of 0.91 V, J_{SC} of 10.84 mA cm^{-2} and FF of 71.11%, leading to a much enhanced PCE of 7.01%. This value is among the highest reported for PSCs based on **PCDTBT:PC_{71}BM** active layer.[38,39] To exclude the influence of methanol treatment,[10,40] a control device without a CIL but with methanol spincoated on the active layer has also been fabricated. Although the methanol-treated device shows superior PCE to that of the device with bare Al, the V_{OC}, J_{SC} and FF of the methanol-treated device are all lower than those of the device with **GQDs-TMA** as the CIL (Table 1). These results confirm the importance of **GQDs-TMA** as the CIL for good PSC device performance. The external quantum efficiency (EQE) curve of the **GQD-TMA** device (Fig. 3b) shows high values above 65% in the range of 460–570 nm, which is consistent with the high J_{SC}

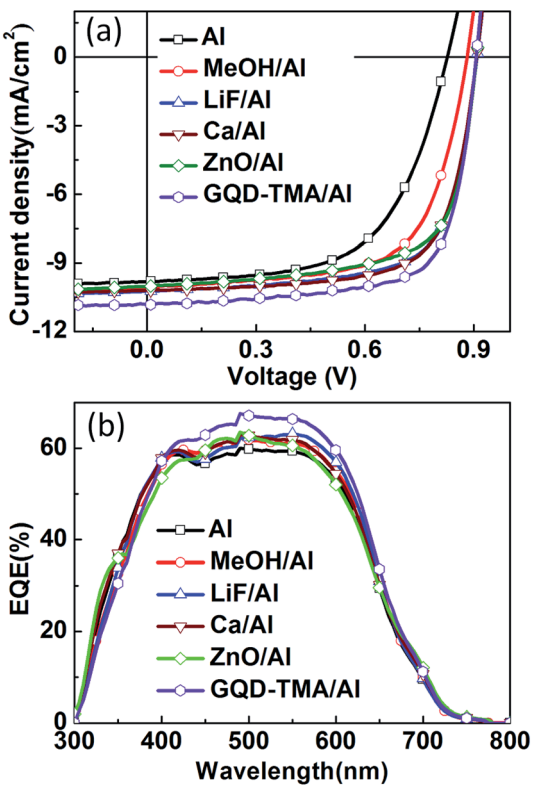

Fig. 3 (a) *J*–*V* plots and (b) EQE curves of the PSC devices with the Al cathode and different CILs.

Table 1 Characteristics of the PSC devices with the Al cathode and different CILs

CIL	V_{OC} (V)	J_{SC} (mA cm^{-2})	FF (%)	PCE_{max} (PCE_{ave}[a]) (%)
None	0.83	9.82	59.45	4.85 (4.75)
With MeOH	0.88	10.10	65.40	5.81 (5.66)
LiF	0.91	10.23	69.19	6.44 (6.30)
Ca	0.91	10.20	69.90	6.49 (6.36)
ZnO	0.91	10.02	68.03	6.20 (6.10)
GQDs-TMA	0.91	10.84	71.11	7.01 (6.86)

[a] The average PCE is obtained over 6 devices.

obtained in the *J–V* plots. We attribute the high V_{OC} and FF to the improved electron extraction and hole blocking with **GQDs-TMA** as the CIL. The low work function of the **GQD-TMA** modified cathode leads to increased built-in potential across the active layer, which improves charge carrier selection and suppresses charge recombination. This is supported by the higher current density under positive bias (>1 V) and much lower current density under reverse bias in the *J–V* plot in the dark (Fig. S4†).[41]

To test of the versatility of **GQDs-TMA**, we fabricated PSC devices based on **GQDs-TMA** with different cathode materials and different active layer materials. As first, PSC devices with **PCDTBT:PC$_{71}$BM** as the active layer and high work function metals as the cathode (Ag and Au) were compared. The *J–V* plots of these devices are shown in Fig. 4a and the parameters are listed in Table S1.† Although the active layers were treated with MeOH, the PSC devices with Ag or Au as the cathode only show a V_{OC} of 0.87 V and 0.80 V, and a PCE of 5.18% and 4.22%, respectively. The low V_{OC} and PCE are due to the non-ohmic contact between the high work function metals with the acceptor **PC$_{71}$BM**. When using **GQDs-TMA** as CILs, the Ag-based and Au-based devices exhibit a V_{OC} of 0.90 V and 0.89 V, respectively, very close to that of the control device with the Al cathode (Fig. 4a). Moreover, the J_{SC} and FF of the Ag/Au-based devices are also obviously improved when using **GQDs-TMA** as the CIL. As a result, the Ag-based and Au-based devices show a much enhanced PCE of 6.26% and 5.41%, respectively. These results suggest that the **GQD-TMA** modified cathode provides an ohmic contact for electron injection despite the high work function of the cathode. This is consistent with the low work functions of Ag and Au after **GQDs-TMA** were spincoated, as estimated from UPS results.

Then we fabricated PSCs based on the highly efficient poly [4,8-bis[(2-ethylhexylthienyl-5-)benzo[1,2-*b*:4,5-*b*′] dithiophene-2,6-diyl][3-fluoro-2-[(2-ethylhexyl)carbonyl]thieno [3,4-*b*] thiophenediyl]] (PTB7-Th):**PC$_{71}$BM** active layer.[42,43] As shown in Fig. 4b, the device with the bare Al cathode with MeOH treatment shows a V_{OC} of 0.74 V, J_{SC} of 17.28 mA cm^{-2}, FF of 58.74% and PCE of 7.51%. In comparison, with **GQDs-TMA** as the CIL, the PCE is greatly improved to 8.80% with a V_{OC} of 0.76 V, J_{SC} of 17.39 mA cm^{-2} and FF of 66.60% (Fig. 4b). This result indicates the good device performance of **GQDs-TMA** as the CIL irrespective of the active layer materials. It is noteworthy that this is

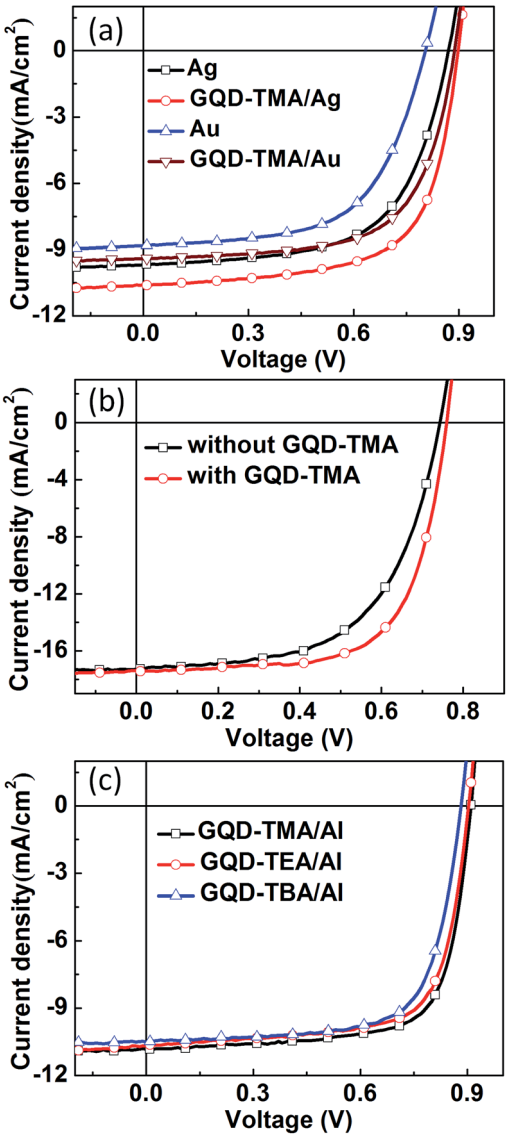

Fig. 4 (a) *J–V* plots of the PSC devices with/without **GQDs-TMA** as the CIL and Ag, Au as the cathode. (b) *J–V* plots of the PSC devices based on the PTB7-Th:**PC$_{71}$BM** active layer with/without **GQDs-TMA** as the CIL. (c) *J–V* plots of the PSC devices with Al as the cathode and **GQDs-TMA**, **GQDs**-TEA or **GQDs**-TBA as the CIL.

the highest PCE for PSCs with graphene materials as the electrode interlayer reported so far.

To further verify the versatility of the material design strategy of **GQDs-TMA**, we prepared tetraethylammonium-functionalized graphene quantum dots (**GQDs**-TEA) and tetrabutylammonium-functionalized graphene quantum dots (**GQDs**-TBA). The alkyl chains in the ammonium groups of **GQDs**-TEA and **GQDs**-TBA are different from that in **GQDs-TMA**. PSC devices with **GQDs**-TEA and **GQDs**-TBA as the CIL were also fabricated and the *J–V* plots under AM 1.5G illumination are shown in Fig. 4c. The parameters are listed in Table S2.† The devices based on **GQDs**-TEA and **GQDs**-TBA CILs exhibit a V_{OC} of 0.88–0.90 V and the PCE of both exceeds 6.5%, indicating that the two materials can also work well as CILs. Therefore, we

think it is a general approach to design CIL materials by incorporating specific polar/ionic groups to the edge of graphene quantum dots. With the increase of the alkyl length (from methyl to *n*-butyl), V_{OC}, J_{SC} and FF of PSCs all decrease gradually, making the PCE decrease slightly from 7.01% to 6.53%. The reason for the weak dependence of the PSC device performance on the alkyl chain length is not clear yet. Possibly, a long alkyl chain length leads to decreased conductivity of the CIL material (Fig. S3†), and consequently results in increased R_S and decreased PCE of the PSC devices (Table S2†).

3. Conclusions

In conclusion, we demonstrate that tetraalkylammonium-functionalized graphene quantum dots can be used as CILs in PSCs for improved device efficiency. The peripheral $COO^-\cdot(CH_3)_4N^+$ groups in **GQDs-TMA** form an interfacial dipole with the metal cathode to decrease the work function. The **GQD** core with a preserved graphene structure gives relatively high conductivity and good film-forming properties. High PCEs of 7.01% and 8.80% have been obtained with **GQDs-TMA** as the CIL for **PCDTBT:PC$_{71}$BM** and PTB7-Th:**PC$_{71}$BM** systems, respectively. These results unambiguously demonstrate that solution-processed graphene materials are a new class of promising interlayers for PSCs with the advantage of low cost.

4. Experimental section

Synthesis of GQDs-TMA, GQDs-TEA and GQDs-TBA

GQDs were synthesized by chemical oxidation of carbon black (Vulcan VXC-72, Cabot Corporation) in HNO_3/H_2SO_4 according to our published procedures.[22] Take **GQDs-TMA** as an example, **GQDs** (50 mg) were first dissolved in water to obtain a homogeneous solution, then tetramethylammonium hydroxide aqueous solution (25 wt%) was added to the **GQD** solution under stirring to give a pH of 7–8. After the water was removed by vacuum distillation, the residual solids were collected and dried under vacuum at 70 °C for 24 hours to give **GQDs-TMA**. Yield: 70 mg. **GQDs**-TEA and **GQDs**-TBA were synthesized using the same method from **GQDs** with tetraethylammonium hydroxide and tetrabutylammonium hydroxide, respectively.

PSC device fabrication and measurement

PCDTBT was synthesized in our laboratory.[44] PTB7-Th (1-material Chemscitech Inc.) and **PC$_{71}$BM** (American Dye Source) were purchased from commercial resources and used as received. ITO glass substrates were ultrasonicated for 10 minutes each sequentially with detergent, de-ionized water, acetone, and iso-propanol, followed by drying at 120 °C in an oven for 2 hours. Before depositing PEDOT:PSS, the ITO substrates were treated with UV–ozone for 25 min. PEDOT:PSS (Clevios VP Al 4083 from H. C. Starck Inc.) was spin-coated on the pre-cleaned ITO substrates at 5000 rpm for 1 min and annealed at 120 °C for 30 min. The substrates were transferred to a nitrogen-filled glovebox. The **PCDTBT:PC$_{71}$BM** (1 : 4 by weight) active layer (75 nm) was spin-coated from the *o*-dichlorobenzene solution. The PTB7-Th:**PC$_{71}$BM** (1 : 1.5 by weight) active layer (100 nm) was spin-coated from the chlorobenzene/1,8-diiodooctane (97 : 3 v/v) solution. The tetraalkylammonium-functionalized graphene quantum dots were dissolved in methanol and spin-coated on top of the active layer at 3000 rpm for 1 min. The thickness was controlled by varying the solution concentration. The optimal thickness is about 3–7 nm. Finally, metal cathodes were deposited, including Al, Ag and Au, in a vacuum chamber with a pressure of about 2×10^{-4} Pa. For the control devices, the other CILs including 20 nm Ca or 1 nm LiF or 30 nm ZnO nanoparticles were deposited between the active layer and metal cathode. The cell active area was 8 mm^2. The *J–V* plots of the devices were measured using a Keithley 2400 source meter under illumination with a light intensity of 100 mW cm^{-2} provided by an Oriel 150 W solar simulator with an AM 1.5G filter. The EQE curves were measured under the short-circuit condition with a lock-in amplifier (SR830, Stanford Research System) at a chopping frequency of 280 Hz during illumination with monochromatic light from a xenon lamp. The thickness of the CILs was determined by profilometry together with the absorbance of the film using the Lambert–Beer law. The conductivity of the different tetraalkylammonium-functionalized graphene quantum dots was calculated from the bulk resistance of samples using Ohm's law ($R = V/I$) with the device structure of ITO/interlayer/Al.

Acknowledgements

The authors are grateful for the financial support from the 973 Project (No. 2014CB643504), the Nature Science Foundation of China (No. 51373165, 51403200), the Strategic Priority Research Program of Chinese Academy of Sciences (No. XDB12010200), and the "Thousand Talents Program" of China.

Notes and references

1 G. Yu, J. Gao, J. C. Hummelen, F. Wudl and A. J. Heeger, *Science*, 1995, **270**, 1789.
2 G. Li, R. Zhu and Y. Yang, *Nat. Photonics*, 2012, **6**, 153.
3 B. C. Thompson and J. M. J. Frechet, *Angew. Chem., Int. Ed.*, 2008, **47**, 58.
4 L. M. Chen, Z. Xu, Z. R. Hong and Y. Yang, *J. Mater. Chem.*, 2010, **20**, 2575.
5 R. Steim, F. R. Kogler and C. J. Brabec, *J. Mater. Chem.*, 2010, **20**, 2499.
6 H.-L. Yip and A. K.-Y. Jen, *Energy Environ. Sci.*, 2012, **5**, 5994.
7 C. C. Chueh, C.-Z. Li and A. K.-Y. Jen, *Energy Environ. Sci.*, 2015, **8**, 1160.
8 Z. C. He, C. M. Zhong, S. J. Su, M. Xu, H. B. Wu and Y. Cao, *Nat. Photonics*, 2012, **6**, 591.
9 C. H. Duan, K. Zhang, C. M. Zhong, F. Huang and Y. Cao, *Chem. Soc. Rev.*, 2013, **42**, 9071.
10 J. H. Seo, A. Gutacker, Y. M. Sun, H. B. Wu, F. Huang, Y. Cao, U. Scherf, A. J. Heeger and G. C. Bazan, *J. Am. Chem. Soc.*, 2011, **133**, 8416.
11 S. H. Liao, Y. L. Li, T. H. Jen, Y. S. Cheng and S. A. Chen, *J. Am. Chem. Soc.*, 2012, **134**, 14271.

12 R. Kang, S. H. Oh and D. Y. Kim, *ACS Appl. Mater. Interfaces*, 2014, **6**, 6227.
13 S. van Reenen, S. Kouijzer, R. A. J. Janssen, M. M. Wienk and M. Kemerink, *Adv. Mater. Interfaces*, 2014, **1**, 1400189.
14 S. J. Liu, K. Zhang, J. M. Lu, J. Zhang, H. L. Yip, F. Huang and Y. Cao, *J. Am. Chem. Soc.*, 2013, **135**, 15326.
15 C. Z. Li, C. Y. Chang, Y. Zang, H. X. Ju, C. C. Chueh, P. W. Liang, N. Cho, D. S. Ginger and A. K.-Y. Jen, *Adv. Mater.*, 2014, **26**, 6262.
16 Z. A. Page, Y. Liu, V. V. Duzhko, T. P. Russell and T. Emrick, *Science*, 2014, **346**, 441.
17 Z.-G. Zhang, B. Qi, Z. Jin, D. Chi, Z. Qi, Y. Li and J. Wang, *Energy Environ. Sci.*, 2014, **7**, 1966.
18 J. Liu, M. Durstock and L. M. Dai, *Energy Environ. Sci.*, 2014, **7**, 1297.
19 J. Liu, Y. H. Xue, Y. X. Gao, D. S. Yu, M. Durstock and L. M. Dai, *Adv. Mater.*, 2012, **24**, 2228.
20 J. Liu, G.-H. Kim, Y. Xue, J. Y. Kim, J.-B. Baek, M. Durstock and L. M. Dai, *Adv. Mater.*, 2014, **26**, 786.
21 J. Liu, Y. H. Xue and L. M. Dai, *J. Phys. Chem. Lett.*, 2012, **3**, 1928.
22 Z. C. Ding, Z. Hao, B. Meng, Z. Y. Xie, J. Liu and L. M. Dai, *Nano Energy*, 2015, **15**, 186.
23 D. Yang, L. Y. Zhou, W. Yu, J. Zhang and C. Li, *Adv. Energy Mater*, 2014, **4**, 1400591.
24 J.-S. Yeo, J.-M. Yun, Y.-S. Jung, D.-Y. Kim, Y.-J. Noh, S.-S. Kimc and S.-I. Na, *J. Mater. Chem. A*, 2014, **2**, 292.
25 M. J. Beliatis, K. K. Gandhi, L. J. Rozanski, R. Rhodes, L. McCafferty, M. R. Alenezi, A. S. Alshammari, C. A. Mills, K. D. G. I. Jayawardena, S. J. Henley and S. R. P. Silva, *Adv. Mater.*, 2014, **26**, 2078.
26 H. B. Yang, Y. Q. Dong, X. Z. Wang, S. Y. Khoo and B. Liu, *ACS Appl. Mater. Interfaces*, 2014, **6**, 1092.
27 F. S. Li, L. J. Kou, W. Chen, C. X. Wu and T. L. Guo, *NPG Asia Mater.*, 2013, **5**, e60.
28 V. Gupta, N. Chaudhary, R. Srivastava, G. D. Sharma, R. Bhardwaj and S. Chand, *J. Am. Chem. Soc.*, 2011, **133**, 9960.
29 L. Tian, D. Ghosh, W. Chen, S. Pradhan, X. J. Chang and S. W. Chen, *Chem. Mater.*, 2009, **21**, 2803.
30 D. Y. Pan, J. C. Zhang, Z. Li and M. H. Wu, *Adv. Mater.*, 2010, **22**, 734.
31 D. J. Ellison, B. Lee, V. Podzorov and C. D. Frisbie, *Adv. Mater.*, 2011, **23**, 502.
32 B. de Boer, A. Hadipour, M. M. Mandoc, T. van Woudenbergh and P. W. M. Blom, *Adv. Mater.*, 2005, **17**, 621.
33 Y. H. Zhou, C. Fuentes-Hernandez, J. Shim, J. Meyer, A. J. Giordano, H. Li, P. Winget, T. Papadopoulos, H. Cheun, J. Kim, M. Fenoll, A. Dindar, W. Haske, E. Najafabadi, T. M. Khan, H. Sojoudi, S. Barlow, S. Graham, J. L. Bredas, S. R. Marder, A. Kahn and B. Kippelen, *Science*, 2012, **336**, 327.
34 Z. C. He, C. Zhang, X. F. Xu, L. J. Zhang, L. Huang, J. W. Chen, H. B. Wu and Y. Cao, *Adv. Mater.*, 2011, **23**, 3086.
35 G. Eda and M. Chhowalla, *Adv. Mater.*, 2010, **22**, 2392.
36 S. H. Park, A. Roy, S. Beaupre, S. Cho, N. Coates, J. S. Moon, D. Moses, M. Leclerc, K. Lee and A. J. Heeger, *Nat. Photonics*, 2009, **3**, 297.
37 J. Liu, S. Y. Shao, G. Fang, B. Meng, Z. Y. Xie and L. X. Wang, *Adv. Mater.*, 2012, **24**, 2774.
38 D. H. Wang, D. Y. Kim, K. W. Choi, J. H. Seo, S. H. Im, J. H. Park, O. O. Park and A. J. Heeger, *Angew. Chem., Int. Ed.*, 2011, **50**, 5519.
39 Z. Xiao, Y. Yuan, B. Yang, J. VanDerslice, J. Chen, O. Dyck, G. Duscher and J. Huang, *Adv. Mater.*, 2014, **26**, 308.
40 H. Q. Zhou, Y. Zhang, J. Seifter, S. D. Collins, C. Luo, G. C. Bazan, T. Q. Nguyen and A. J. Heeger, *Adv. Mater.*, 2013, **25**, 1646.
41 J. D. Servaites, M. A. Ratner and T. J. Marks, *Energy Environ. Sci.*, 2011, **4**, 4410.
42 S. H. Liao, H. J. Jhuo, Y. S. Cheng and S. A. Chen, *Adv. Mater.*, 2013, **25**, 4766.
43 Z. C. He, B. Xiao, F. Liu, H. B. Wu, Y. L. Yang, S. Xiao, C. Wang, T. P. Russell and Y. Cao, *Nat. Photonics*, 2015, **9**, 174.
44 B. Meng, Y. Y. Fu, Z. Y. Xie, J. Liu and L. X. Wang, *Macromolecules*, 2014, **47**, 6246.

